Journal of Microscopy, Vol. 163, *Pt* 1, *July* 1991, *pp.* 51–64.
Received 29 *October* 1990; *revised and accepted* 19 *January* 1991

ADONIS0022272091000873

Platinum/iridium/carbon: a high-resolution shadowing material for TEM, STM and SEM of biological macromolecular structures

by ROGER WEPF*, MATTHIAS AMREIN*, URS BÜRKLI† *and* HEINZ GROSS*,
**Institute for Cell Biology, Swiss Federal Institute of Technology, ETH-Hönggerberg,* 8093 *Zürich, Switzerland and* †*SULZER-Innotec Material and Surface Engineering,* 8404 *Winterthur, Switzerland*

KEY WORDS. High-resolution shadowing, platinum/iridium/carbon, freeze-drying, polyhead surface structure, HPI-layer, FESEM, STM, TEM, WDX-analysis.

SUMMARY

Thin Pt/Ir/C coating films (1·5 nm) show a fine granularity and provide a high structural resolution in the transmission electron microscope (TEM) when applied to freeze-dried biological macromolecules. They keep their structure when exposed to atmospheric conditions, without the need of an additional stabilizing carbon layer, in contrast to conventional high-resolution shadowing materials such as Ta/W and Pt/C. However, the correct ratio of the components has turned out to be crucial. When evaporating Pt/Ir/C from the source electrode in an electron-beam-heated evaporator, the ratio of the three elements changes progressively, and, consequently, the properties of such films depend strongly on the mass that has been pre-evaporated.

In this paper we present a quantitative analysis of the composition of Pt/Ir/C films by wavelength-dispersive X-ray analysis (WDX) undertaken in association with TEM experiments. We applied Pt/Ir/C shadowing to two regular biological test specimens, the phage T4 type III polyhead and the HPI-layer of *Deinococcus radiodurans*. It turns out that Pt/Ir/C films containing at least 25% C are three-dimensionally stable on the freeze-dried macromolecular samples.

By the dramatically improved resolution power of the latest scanning electron microscopes (SEM) and the invention of the scanning tunnelling microscope (STM), two new surface-sensitive tools for the investigation of biological macromolecular structures became available. The Pt/Ir/C coating has proved to be well suited for STM and SEM imaging of freeze-dried biological structures because of its good electrical conductivity and its direct three-dimensional stability. We compare STM, SEM and TEM images of freeze-dried and Pt/Ir/C-coated polyheads.

INTRODUCTION

Metal shadowing was the first method of contrast enhancement practiced in biological transmission electron microscopy (TEM) (Mahl, 1942; Müller, 1942; Williams & Wyckoff, 1944), and it has been used in scanning electron microscopy (SEM) from the beginning of its biological application (Smith & Oatley, 1955; Echlin, 1968). Recently, metal coating has also been used in scanning tunnelling microscopy

(STM) for research into the structure of biological macromolecules (e.g. Amrein *et al.*, 1988; Guckenberger *et al.*, 1988; Zasadzinsky *et al.*, 1988; Stemmer *et al.*, 1989).

Since the introduction of heavy-metal shadowing in electron microscopy, it has become well known that the resolution is limited by the granularity of the coating films (for reviews see Reimer, 1967; Venables *et al.*, 1984; Gross *et al.*, 1985). Knoch & König (1956) first showed that the incorporation of carbon (C) into platinum (Pt) films reveals finer granular, though still highly contrasting films when compared to the pure metal films. Such films are attained by simultaneously evaporating platinum and carbon (Bradley, 1958). A further reduction of the grain size can be achieved by increasing the amount of carbon by evaporating iridium together with platinum and carbon. However, when first invented by Skatulla & Horn (1960), no significant difference could be found between Pt/C and Pt/Ir/C films. This may have been due to the relatively simple shadowing technique used or the poor performance of the current TEMs. Coating at very low specimen temperature (20 K) also helps to reduce the grain size of shadowing films (Gross *et al.*, 1985). Besides heavy-metal–carbon compounds, tantalum/tungsten (Ta/W) is a frequently used high-resolution shadowing material in TEM of biological structures (Bachmann *et al.*, 1969; Gross *et al.*, 1985).

The dramatically improved resolution power of the latest SEMs and the invention of the STM have added two new surface-sensitive tools for the investigation of biological macromolecular structures. Until now SEM has been an established method for visualizing surface details down to a resolution of 5 nm at most (for a review see McMullen, 1989). The introduction of the field-emission electron sources and newly designed lenses have made field-emission scanning electron microscopes (FESEM) available which have a resolution power better than 1 nm (Nagatani *et al.*, 1987). The SEM enables the visualization of surfaces of large bulk specimens from low to high magnification up to macromolecular dimensions (Peters, 1986; Walther & Hentschel, 1989). Usually, SEM requires electrically conductive surfaces. This can be achieved by coating the surfaces with a conductive film. Up to now, the most frequently used coating films for high-resolution secondary imaging have been chromium for secondary electron (SE) imaging (for a review see Peters, 1986) and Pt/C for backscattered electron imaging (Walther & Hentschel, 1989).

STM is an established method for probing the surface of metals and semiconductors, structurally and electronically, to an atomic scale. The ability of STM to reveal directly the three-dimensional (3-D) structure of a surface with high resolution makes it attractive in biological molecular structure research. However, STM of biological material is hampered due to its poor intrinsic electrical conductivity. Resorting to conductive coating films (Amrein *et al.*, 1989) or metal replicas (Zasadzinsky *et al.*, 1988) makes it relatively easy to obtain reproducible trustworthy images that are not influenced by the intrinsic conductivity properties of the biological macromolecular structures.

The metal coat is applied not only in order to enhance the contrast in TEM and SEM and to render the surface conductive for STM and SEM, it also must stabilize the protein in the close-to-native conformation that has been preserved by careful freeze-drying of the sample (Gross, 1987). Metal coats such as Ta/W and Pt/C, commonly used as high-resolution shadowing materials in TEM, need an additional carbon layer in order to maintain their 3-D shape and fine granular structure when exposed to atmospheric conditions (Bachmann & Hilbrand, 1965). Such a carbon-backing layer, however, blurs fine surface features when probed by an STM and suppresses the SE signal from the metal film in an SEM. Shadowing without an additional carbon layer is also of interest for TEM applications because carbon may contribute disturbingly to the metal contrast in projection. Pt/Ir/C films have been shown to remain three-dimensionally stable when transferred to atmospheric conditions after freeze-drying

the sample. They allow stable tunnelling and provide good contrast in SEM, as well as in TEM. However, the correct ratio of the components has proved to be crucial when a fine granular, three-dimensionally stable coating is required.

We quantified the composition of Pt/Ir/C films that were prepared in parallel to samples for the TEM, by wavelength-dispersive X-ray analysis (WDX). In order to study the 3-D stability and resolution power of Pt/Ir/C films in TEM, SEM and STM we used bacteriophage T4 type III polyheads as a test specimen. The polyheads are composed of capsomeres arranged on a near-hexagonal lattice which is folded into a cylinder. When adsorbed to a support film, the spread-flattened tubes allow for standard correlation averaging (Saxton & Baumeister, 1982), to determine the detailed structure of the capsomeres. The type III polyheads have quasi-*p*6 symmetry and a lattice constant of 13 nm (Steven *et al.*, 1976). The 3-D stability of the Pt/Ir/C films was further verified on the HPI-layer, a regular protein monolayer much more strongly corrugated than the polyheads (Baumeister *et al.*, 1982). Finally, STM, TEM and SEM data of freeze dried, Pt/Ir/C-coated polyheads are compared.

MATERIALS AND METHODS

Pt/Ir/C electrodes

We used a Pt/Ir cylinder (diameter = 1·5 mm, length = 1·5 mm, 70% Ir; Heraeus) inserted into a graphite rod (diameter = 2 mm) as an evaporation source (Fig. 1a). From this electrode a mass of 13·8 mg had to be evaporated prior to coating of the biological sample in order to obtain three-dimensionally stable Pt/Ir/C films. The electrodes were treated in the following way: the mass of a new Pt/Ir/C electrode was determined on a balance with a precision of 0·01 mg; it then was carefully mounted in an electron-beam-heated gun (Fig. 1b). Evaporation of the Pt/Ir/C was carried out in a freeze-etch unit (BAF400T, Balzers) at a pressure of 2×10^{-3} Pa by applying a high tension of about 1800 V and an emission of about 50 mA. The emission was raised slowly in order to allow the Pt/Ir cylinder to melt into the carbon rod. Sparks emerging from the gun indicated that the evaporation had begun. From the electrode, 13 $\mu g/cm^2$ (650 Hz), measured on a quartz crystal thickness monitor (QSG 201D, Balzers), was evaporated. The quartz crystal was mounted perpendicular to the shadowing direction at the sample plane, in a distance of 15 cm from the source electrode. The rate of evaporation was kept within 0·04 $\mu g/cm^2/s$ (2 Hz/s) to 0·24 $\mu g/cm^2/s$ (12 Hz/s); higher rates were avoided by regulating either the high tension or the emission. Then the electrode was weighed again in order to determine the evaporated mass, usually about 13 mg. This implies that 0·1 mg of the electrode corresponds to about 0·1 $\mu g/cm^2$ (5 Hz) measured on the quartz crystal monitor. The remaining difference to the required mass loss of 13·8 mg was evaporated onto a shutter just before coating of the biological specimen.

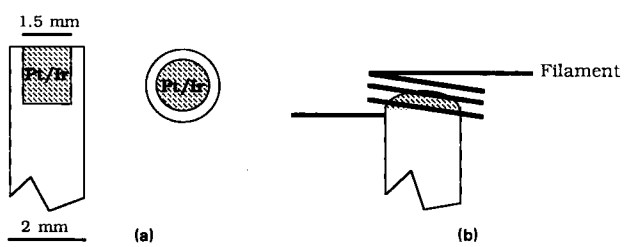

Fig. 1. (a) Pt/Ir/C electrode, composed of a platinum–iridium (30%/70%) cylinder inserted in a carbon rod. (b) Position of the Pt/Ir/C electrode relative to the tungsten cathode of the electron-beam-heated gun.

WDX analysis

Pt/Ir/C samples were collected on polished (3-μm diamonds) Fe and Al surfaces (99·95% purity, Materials Research S.A.). The films were collected five times nearer the evaporation source than the biological sample in order to obtain films thick enough for WDX analysis (approximately 80 nm). The mass of the Pt/Ir/C films was about 75 $\mu g/cm^2$ corresponding to 3 $\mu g/cm^2$ (150 Hz) at the specimen plane. Fe and Al were chosen because these elements have no overlap in the energy of the emitted X-ray radiation with Pt, Ir and C. In addition, Al allows for optimal absorption correction for Pt, Ir and C measurements. The absorption correction is particularly important in WDX measurements of thin films (Oda & Nakajima, 1975).

The Pt/Ir/C samples were analysed in an M9 microprobe (Cambridge Instruments) at an acceleration voltage of 20 kV for Pt and Ir measurements, and 15 kV for C, Fe and Al measurements. The microprobe was equipped with a xenon detector for Pt, Ir and Fe measurements and with a flow-counter (argon methane) for C and Al measurements. For X-ray reflections the microprobe was equipped with lithium-fluoride crystals (for Pt, Ir and Fe signals), with PET crystals (Al) and with Pb-stearat crystals (C). The probe current was 20 nA for Pt and Ir and 100 nA for Al, Fe and C. On each sample at least three different areas (80 × 100 μm) were analysed for 40 s per area.

In addition to the film measurements, the elemental distribution in a cross-section of the melting zone of the Pt/Ir/C electrode, after a pre-evaporation of 13·8 mg of material, was determined. In order to do so the electrode was embedded in a copper resin (Struers: mounting resin-2) and then rubbed and polished (5-μm diamonds) down to the central section. Analysis of the section across the evaporation electrode was performed using similar conditions as for the films. Measurements were carried out in steps of 50 μm for Pt and Ir and in steps of 100 μm for C, beginning at the top of the electrode towards the end of the insert.

Sample preparation

HPI-layer sheets from the bacterium *Deinococcus radiodurans* were isolated as described by Baumeister *et al.* (1982) and bacteriophage T4 type III polyheads were prepared as described by Steven *et al.* (1976). For TEM and SEM samples, carbon films (8 nm) mounted on copper grids (400 mesh/in.) were used as support. For STM, the specimens were adsorbed on thin mica platelets covered with a Pt/C film (2 nm) (Amrein *et al.*, 1989). Prior to adsorption, the support films were rendered hydrophilic (glow discharged) in a Harrick Plasma cleaner. Samples were diluted with double-distilled water prior to adsorbing them for 1 min to the support film by placing it upside down onto a 5-μl sample drop. The grids were then washed with double-distilled water, excess water was removed and the grids were immediately frozen by dipping them into liquid nitrogen. While submersed in liquid nitrogen they were fixed on the specimen table of the ultrahigh-vacuum (UHV) machine (Balzers, BAF 500K) and transferred to the pre-cooled cold-stage of the airlock of the UHV machine by using the counter-flow loading device. Freeze-drying was carried out for 2–4 h at 193 K under high-vacuum conditions ($< 10^{-4}$ Pa) in the airlock. For shadowing, the specimen table was transferred into the pre-cooled (193 K) specimen stage of the UHV chamber (2×10^{-7} Pa). TEM samples were rotary shadowed with Pt/C, Pt/Ir/C or Ta/W. Film thickness and deposition rate were continuously measured with a quartz crystal film monitor and a rate meter (Balzers QSG 301, QRG 301). The deposition onto the specimen was monitored by a pneumatic, cooled shutter. The Ta/W films were immediately stabilized with a 5-nm-thick carbon backing layer. For SEM and STM the specimens were rotary shadowed with Pt/Ir/C from 65° elevation. The specimen temperature was kept at 20 K during shadowing except for the comparison in Figs. 2 and 9, where the

specimen temperature was 193 K. After shadowing, the samples were warmed to room temperature and withdrawn from the vacuum.

TEM and SEM recording

TEM samples were investigated in a Philips CM 12 electron microscope operated at an acceleration voltage of 100 kV and equipped with a low-dose unit. The micrographs were recorded at a nominal magnification of 45,000 and about 450 nm underfocus on Agfa-Gevaert Scientia film (23D56 P3 AH). The magnification was calibrated with the known lattice constant of the test specimens.

The samples prepared for TEM were also investigated in an FESEM (Hitachi S-900) equipped with a Gatan cryo-specimen holder, at an acceleration voltage of 30 kV. The object temperature in the microscope was kept within 170–180 K. The SE images were recorded on Kodak T-Max 400. Irradiation damage and contamination was kept small by selecting an area of interest at a magnification of 20–30,000 prior to recording it at a magnification of 110,000. The focus was adjusted during the first scan lines.

STM measurement

STM measurements were performed under atmospheric conditions with a pocket-sized microscope (Gerber *et al.*, 1986) in the constant current mode as described by Amrein *et al.* (1989).

Digital image processing and optical diffraction

The TEM and SEM micrographs were screened and selected for best resolution in a light-optical diffractometer and the diffraction patterns were recorded on 35-mm film (Ilford FP 4). In addition, the diffraction pattern allows micrographs which show drift or astigmatism to be eliminated. Selected micrographs were digitized on an Optronics-P1700 HS photoscanner using a raster of $(25\ \mu m)^2$, corresponding to 0·52 nm for TEM and 0·36 nm for SEM micrographs at the specimen scale. Correlation averaging was applied to 512×512 pixels (HPI-layer) or 1024×256 pixels (polyheads), using the Semper 6 (Synoptics) software, installed on a Personal Iris (Silicon Graphics). Averaged images were recorded directly from the monitor on 35-mm film (Ilford Pan F). STM images were processed as described by Amrein *et al.* (1989).

RESULTS AND DISCUSSION

Properties of Pt/Ir/C films

When evaporating Pt/Ir/C from a new source electrode, the ratio of the three elements changes progressively and, consequently, the properties of such films depend strongly on the mass that has been pre-evaporated from the source electrode. The granularity becomes finer with an increasing amount of material pre-evaporated, and the films gain 3-D stability.

From TEM experiments, made in parallel to WDX of samples (Fig. 5), we learned that Pt/Ir/C films containing at least 25% carbon are three-dimensionally stable when transferred to atmospheric conditions after freeze-drying the sample. Figure 2(a) shows a micrograph of a T4 type III polyhead freeze-dried and rotary shadowed with Pt/Ir/C from an elevation angle of 30°. The hexagonal arrangement of the capsomeres that compose the polyhead is resolved by the Pt/Ir/C film even in the raw data. In the corresponding averaged image the capsomere appears as a hexameric structure. Connections between the protomers of neighbouring capsomeres are just visible.

Almost identical results are obtained after shadowing with Ta/W (Fig. 2c). Here the finest details, the connections between the protomers, appear with an even better contrast. Note, however, that Ta/W requires a stabilizing carbon layer which makes it unsuitable for SEM and STM applications.

Pt/Ir/C films containing less than 25% carbon have a significantly rougher

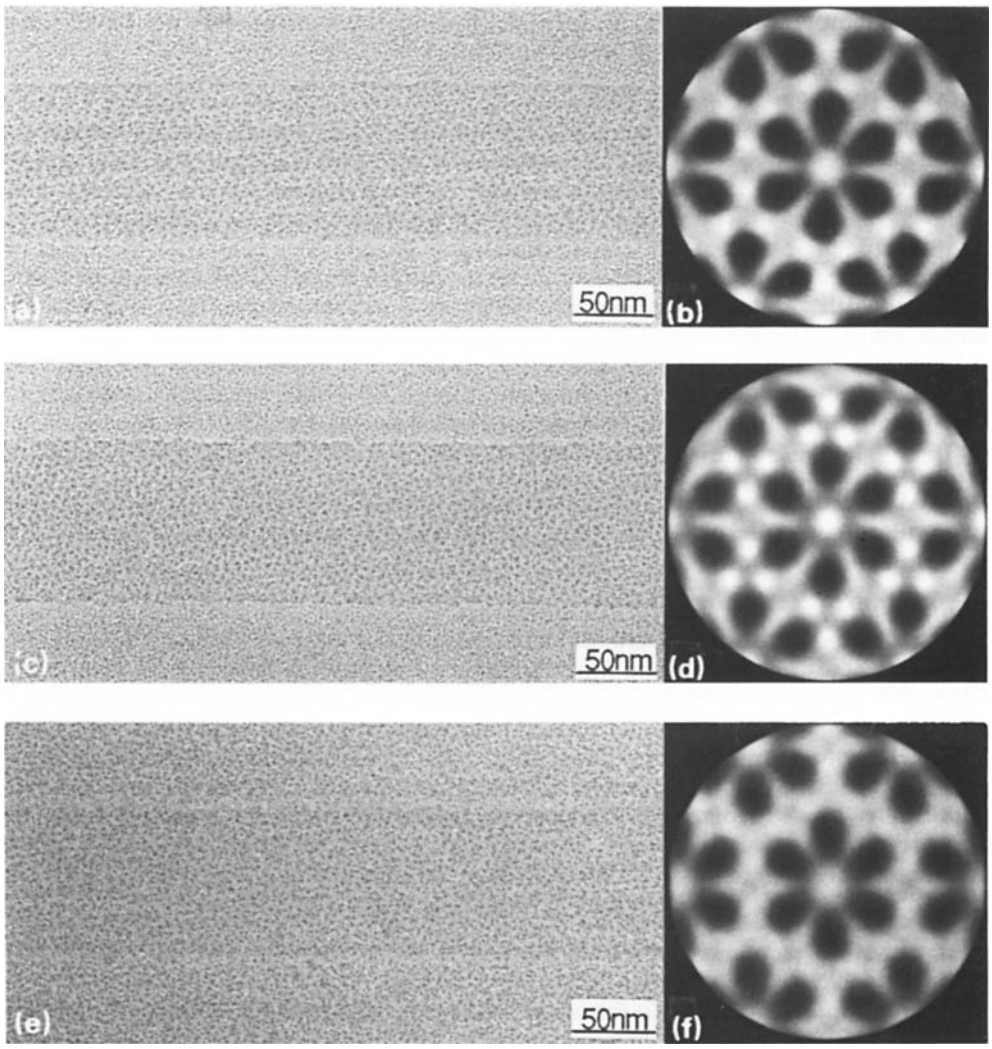

Fig. 2. TEM micrographs of a freeze-dried polyhead, rotary shadowed at an elevation angle of 30°, with: (a) 1·5 mm Pt/Ir/C, (c) 0·7 nm Ta/W, (e) 0·7 nm Pt/C. In (a), the film resolves the hexagonal arrangement of the capsomeres that compose the polyhead. The corresponding correlation averaged images are shown in (b), (d) and (f). (b) A hexameric capsomere structure. Fine connections between the protomers of different capsomeres indicate the high resolution power of Pt/Ir/C films. (d) The same structural features are obtained after correlation averaging. (f) The capsomere structure is poorly revealed after correlation averaging.

granularity, similar to that of Pt/C films (Fig. 2e). The hexagonal lattice appears less clear in the micrograph and the averaged capsomere merely shows six globules with no finer structural features resolved.

From TEM (Buhle *et al.*, 1985) and STM measurements (Amrein *et al.*, 1989) it is known that polyheads have a rather smooth surface relief. In order to investigate the stability of Pt/Ir/C films on more corrugated objects, we used the HPI-layer (hexagonally packed intermediate layer) as a test specimen. The HPI-layer is a loosely packed regular protein monolayer (RS-layer) found in the cell wall of the bacterium *Deinococcus radiodurans* (Baumeister *et al.*, 1982). 3-D models of the HPI-layer have been obtained by electron microscopy (Baumeister *et al.*, 1986; Gross, 1987;

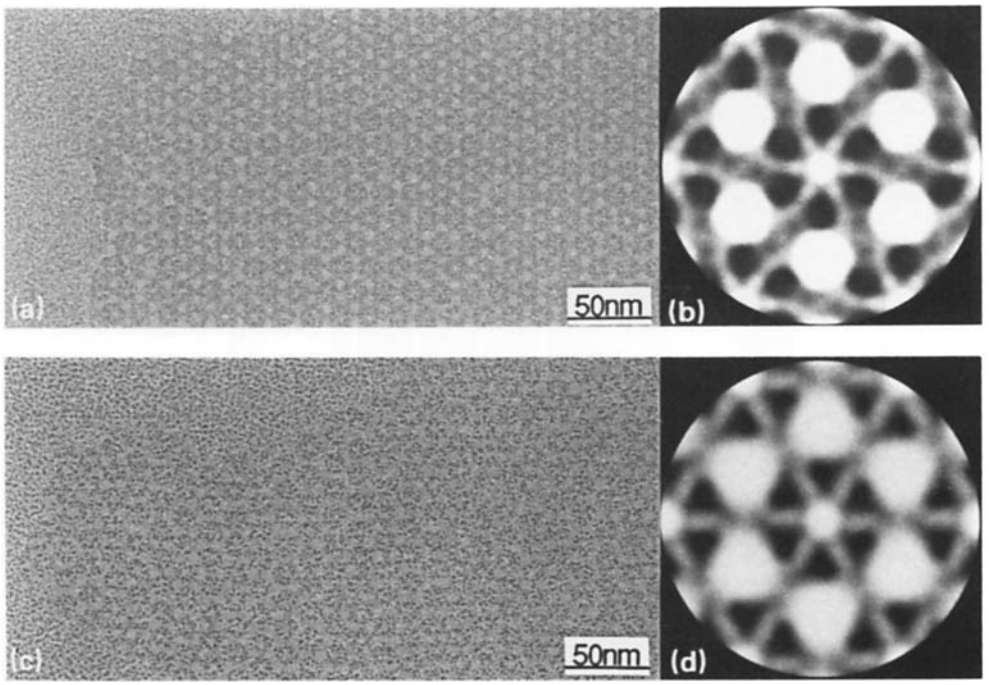

Fig. 3. TEM micrographs and the corresponding averaged images of freeze-dried HPI-layer, rotary shadowed at an elevation angle of 30° with either Pt/Ir/C (a,b) or Pt/C (c,d). The Pt/Ir/C coating reveals the HPI-layer topology in a detailed way. Note the handedness of the core and the separation on the interconnecting spokes. The freeze-dried state of the structure seems to be well preserved. Pt/C without carbon backing, on the other hand, reveals the HPI-structure very poorly. Apparently, Pt accumulates preferentially on the HPI-layer core region. Most probably, this reorganization of Pt is caused by a structural collapse during rehydration of the freeze-dried structure when it is exposed to atmospheric conditions.

Jakubowski *et al.*, 1988) and by tunnelling microscopy. The HPI-layer has *p*6 symmetry and a lattice constant of 18 nm. Most of the protein mass of the hexameric complexes is concentrated in a core-like region from which interconnecting spokes emanate. The core is surrounded by relatively large holes.

A comparison between Pt/C- and Pt/Ir/C-shadowed, freeze-dried HPI-layers is shown in Fig. 3. Here the structural resolution is indeed much more strongly affected by the choice of the coating material than in case of the polyheads. Correlation averaging of the Pt/Ir/C-coated HPI-layer reveals that the core is subdivided into six prominent and well-separated peaks. The interconnecting spokes show a distinct handedness and appear to be composed of two subunits. The resolved surface structure is in good agreement with the 3-D models obtained by tilt-series reconstruction (Jakubowski *et al.*, 1988) and by relief reconstruction (Gross, 1987). On the other hand, Pt/C without carbon backing reveals the HPI-layer structure very poorly. The metal seems to be preferentially accumulated on the core subunits and hardly any metal is found on the spokes. The rough granularity of such Pt/C films on freeze-dried surfaces most probably is caused by a structural collapse during rehydration under atmospheric conditions (compare also Fig. 2). In Pt/Ir/C films, on the other hand, such cluster formation is suppressed by the greater amount of carbon that acts as a stabilizing matrix for the metal coating.

Excellent structural preservation has also been obtained on freeze-dried and Pt/Ir/C-coated creatine kinase (Winkler *et al.*, 1991) and on lipid–porin membranes (Hoenger *et al.*, 1990).

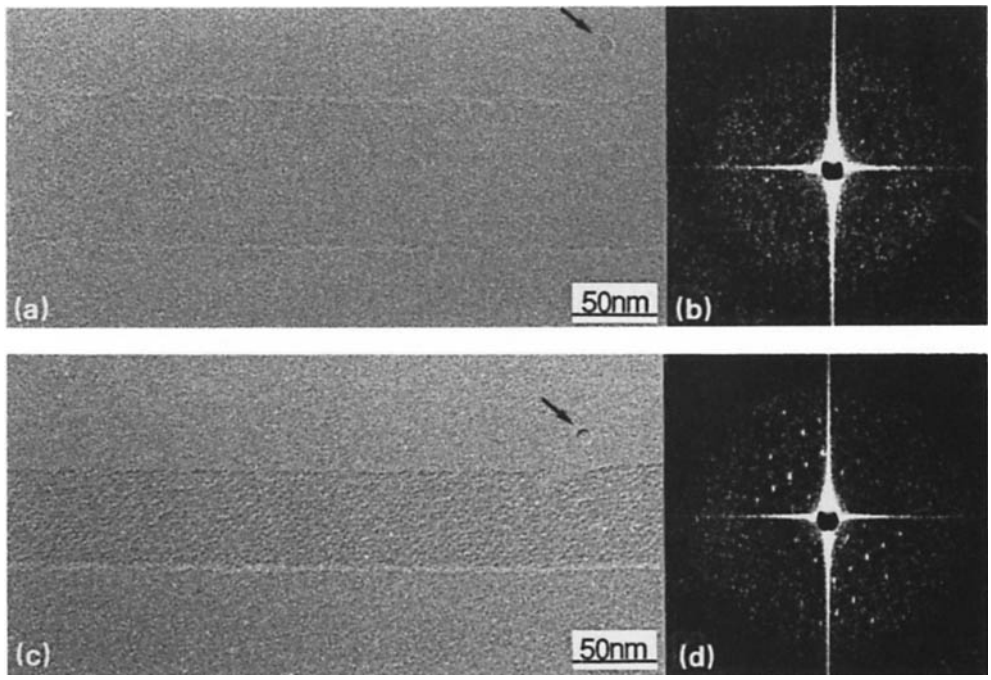

Fig. 4. In order to investigate if Pt/Ir/C accumulates at preferential sites, freeze-dried polyheads were coated at an elevation angle of 90°, where any shadow casting is absent. Indeed, in TEM projection of an untilted polyhead (a), no contrast is revealed beside a faint contour of the borders. The absence of a significant periodic signal in the optical diffraction pattern (b) indicates that no significant decoration has occurred. If the same polyhead is imaged at a tilt angle of 55° the periodic structure is clearly revealed. The corresponding diffraction pattern proves that the periodic surface relief is well preserved.

Surprisingly, Pt/Ir/C shadowing films, on freeze-dried biological macromolecules, that contain at least 25% carbon are stable under electron irradiation within a range of 1200–80,000 e^-/nm^2.

Decoration

Shadowing materials often tend to accumulate at preferred sites on biological specimens (decoration) and hence, in a TEM projection, the contrast due to the shadow casting is superimposed on the contrast caused by the decoration (Bachmann *et al.*, 1985; Winkler *et al.*, 1985). In order to investigate preferential nucleation of Pt/Ir/C, we coated the polyheads at an elevation angle of 90° (Fig. 4). Here shadow casting is basically absent and therefore no contrast should be observed in an untilted projection. Indeed, virtually nothing can be seen on the micrograph (Fig. 4a) except the faint contour of the polyhead borders. The corresponding optical diffraction pattern reveals no significant periodic signal, indicating that decoration effects are basically absent. When the same polyhead is viewed tilted with respect to the coating direction, the periodic structure is revealed by its relief contrast (Fig. 4c). The diffraction pattern proves that the periodic surface relief of the polyhead is well preserved.

Composition of Pt/Ir/C films

The composition of Pt/Ir/C films (Fig. 5a), sequentially collected from a new source electrode, was quantified by WDX. The mass of the different Pt/Ir/C films was kept constant. At the start, Pt/Ir/C films contain 80% platinum, 5% iridium and 15%

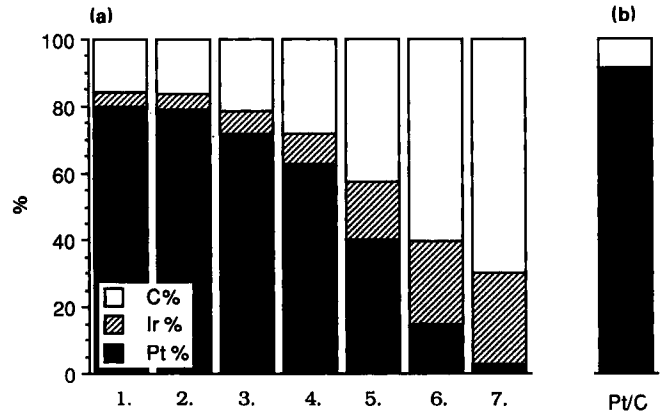

Fig. 5. (a) WDX analysis of Pt/Ir/C films, sequentially collected from a new evaporation source. The first film is collected within a range of 6–9 $\mu g/cm^2$, the second from 9–12 $\mu g/cm^2$, etc., measured at the specimen plan. This corresponds to a 6–9-mg and a 9–12-mg mass evaporated from the source electrode, respectively. The ratio of Pt, Ir and C changes upon the evaporation of the mass from the source. The Pt content decreases continuously, while the Ir and C content increases. In Pt/C films (b), the carbon content is significantly smaller than in Pt/Ir/C films.

carbon. Here the ratio of metal to carbon is in the range that is observed in pure Pt/C films (Fig. 5b). Subsequently the amount of platinum decreases, while carbon and iridium increase.

Pt/Ir/C films that contain just enough carbon to be three-dimensionally stable (25%) have been reproducibly achieved after pre-evaporation of at least 13 $\mu g/cm^2$ (650 Hz), measured with a quartz crystal monitor, from a new source electrode (Fig. 6). We usually pre-evaporated 14 $\mu g/cm^2$ (700 Hz) to ensure we obtained stable films. However, the quartz crystal measurement is a relative mass measure which may vary in different freeze-etch units. Therefore we established a general criterion, namely the determination of the mass loss by the pre-treatment of a new source electrode. In our freeze-etch unit, 14 $\mu g/cm^2$ (700 Hz) corresponded to $13{\cdot}8 \pm 0{\cdot}39$ mg of material evaporated from the source electrode. Mass measurements were performed on twenty-

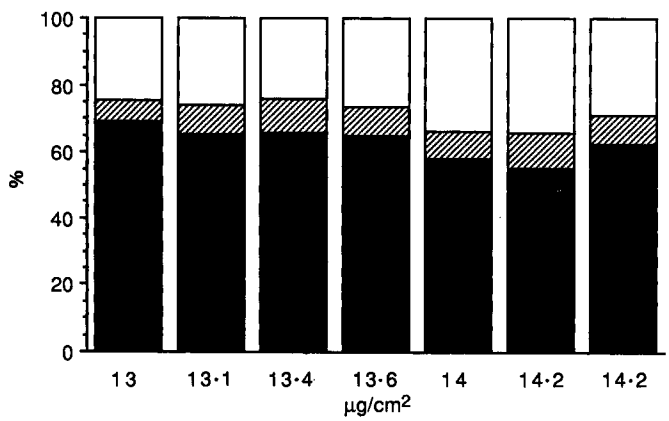

Fig. 6. WDX analysis of Pt/Ir/C films after a pre-evaporation of at least 13 $\mu g/cm^2$ (650 Hz) from the Pt/Ir/C electrode. Note that the carbon content of at least 25%, required for stable and fine granular films, is reproducibly attained after a pre-evaporation of 14 $\mu g/cm^2$ (700 Hz) from a new source electrode. 14 $\mu g/cm^2$ (700 Hz) corresponds to a 13·8-mg mass evaporated from a new Pt/Ir/C source.

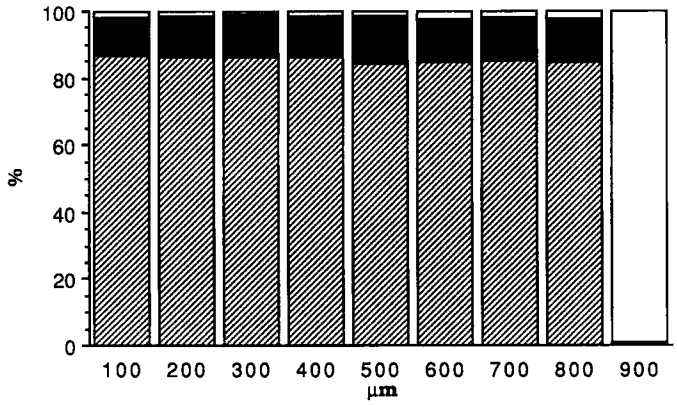

Fig. 7. An analysis of a cross-section through the melting zone of a Pt/Ir/C electrode after a pre-evaporation of 13·7 mg. Interestingly the composition of the melting zone (12·7% Pt, 85·5% Ir and 1·7% C) differs distinctively from that of the corresponding Pt/Ir/C film (Fig. 6). This means that Pt evaporates preferentially from the electrode.

three electrodes. The standard deviation of the carbon content is 3·6% for identical pre-treatment.

Interestingly, the composition of the evaporated films differs distinctively from that of the solidified melting zone of the Pt/Ir/C electrode. An analysis of a section across the melting zone of an electrode after pre-evaporation of 13·7 mg is shown in Fig. 7. No significant gradient of platinum, iridium or carbon could be found within the melting zone. The averaged composition is $12{\cdot}7 \pm 0{\cdot}7\%$ Pt, $85{\cdot}5 \pm 0{\cdot}9\%$ Ir and $1{\cdot}7 \pm 0{\cdot}5\%$ C. The enrichment of iridium with respect to a new electrode proves that platinum evaporates preferentially according to the higher saturation vapour pressure. The carbon content of the Pt/Ir/C films is determined by the iridium content of the electrode. Most probably the evaporated carbon is diluted in the Pt/Ir melting zone.

The thickness of Pt/Ir/C films is not directly obtainable since the density of the films at a certain composition is not precisely known. STM measurements of the used Pt/Ir/C film (1·4 $\mu g/cm^2$, 70 Hz) revealed a film thickness of 1·4–1·5 nm.

Application of Pt/Ir/C films for TEM, SEM and STM

The fine granular structure, the good electrical conductivity and the 3-D stability at only about 1·5 nm thickness of Pt/Ir/C films make them ideal for SEM and STM imaging of biological macromolecular structures. For SEM it is important to have a

Fig. 8. (a) Raw STM data of a polyhead, freeze-dried and Pt/Ir/C-coated (1·5 nm) at an elevation angle of 65°. Note that the capsomeres can be distinguished as hexamers even in the raw data. The averaged capsomere morphology is shown in (c) as a plan view, and in (b) as a section along a line through the centre of the capsomere and the tops of two protomers. The capsomere is composed of six protomers and has a capsomere orientation angle ϕ of approximately 30°.

Fig. 9. TEM micrograph of freeze-dried polyheads Pt/Ir/C shadowed (1·5 nm) at an elevation angle of 30°. The averaged structure shows connections between different protomers, a Y-shaped connection on the threefold axis (3) and an X-shaped connection on the twofold axis (2). These structures most probably belong to the lower part of the polyhead relief since they are not visible in the STM. The capsomere orientation angle is 31°.

Fig. 10. (a) SE image of a polyhead, freeze-dried and Pt/Ir/C coated (1·5 nm) at an elevation angle of 65° and recorded in an in-lens type FESEM. The capsomeres are just visible. Note the granular appearance of the coating film which may be due to particle contrast of single metal grains incorporated in a diffuse carbon matrix. The unsymmetrical averaged image of the capsomere (b) shows the six protomers and faint Y-shaped connections on the threefold axis. The highly symmetrical quality of the SE-image allows us to symmetrize the averaged structure (c).

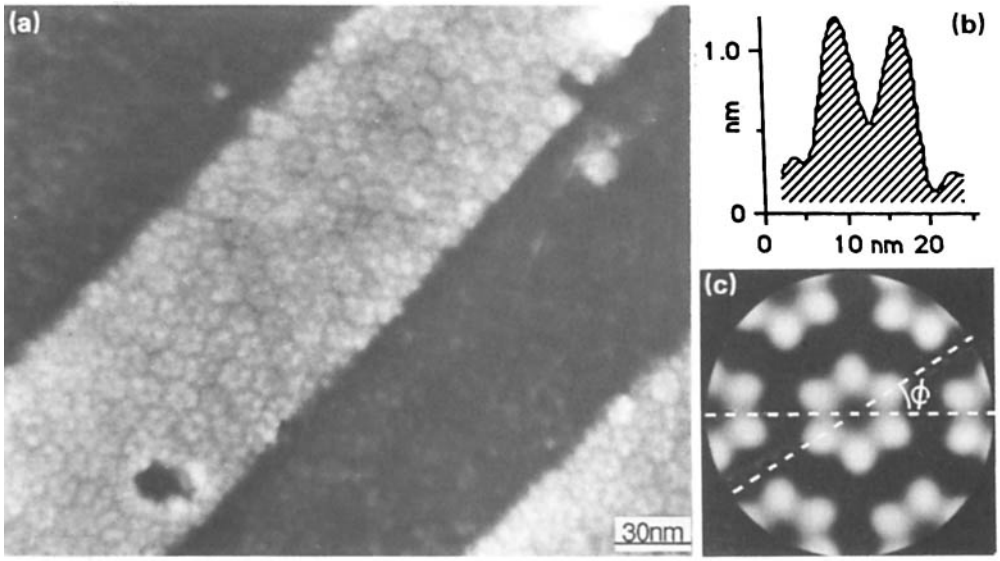

Fig. 8.

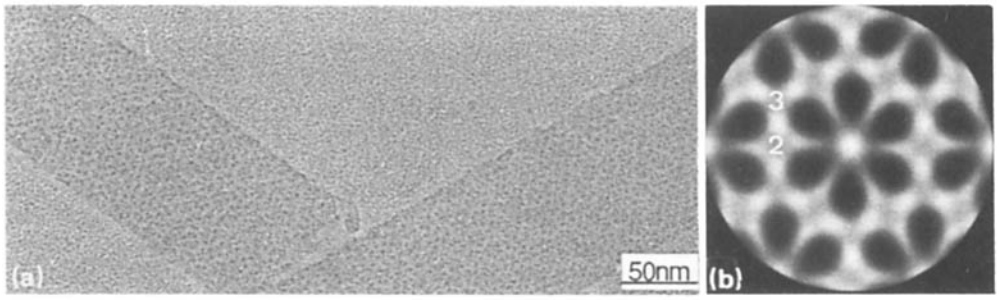

Fig. 9.

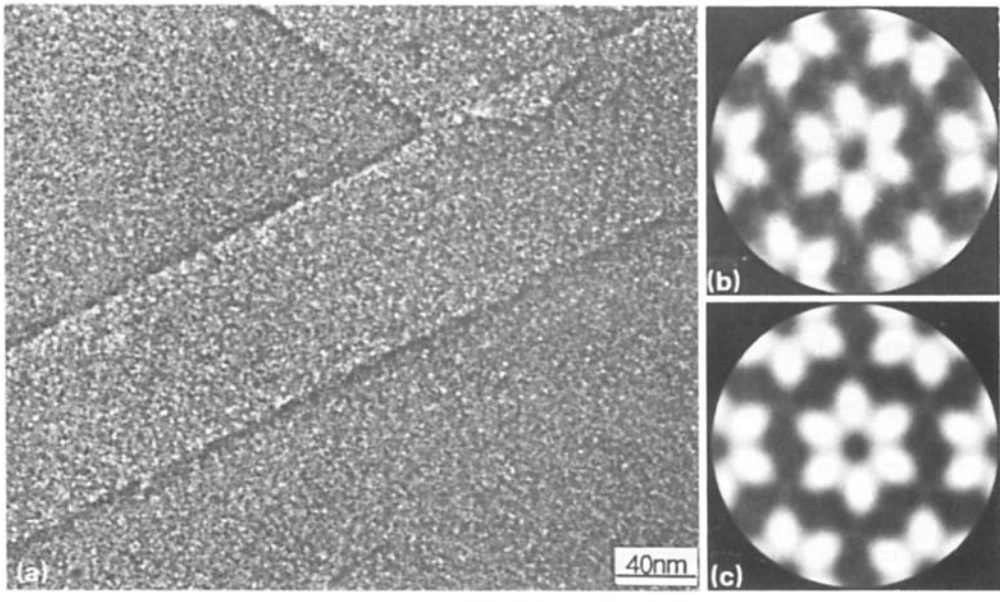

Fig. 10.

conducting film with a small electron-free pathway or a minimized lateral scattering to obtain a well-located signal. The high conductivity of the Pt/Ir/C coating results in reproducible STM images that are not influenced by the intrinsic conductivity properties of the biological structures.

In the following we show TEM, STM and SEM images of freeze-dried polyheads coated with Pt/Ir/C. For STM and SEM the polyheads were rotary shadowed at an elevation angle of 65° in order to achieve a homogeneous, coherent coating. Figure 8(a) shows raw STM data after subtraction of a least-squares fitted plane. The morphological units, the capsomeres, can easily be distinguished. The capsomere morphology obtained by correlation averaging reveals a hexamer with the peaks of its protomers lying on a circle with a diameter of 8 nm. The capsomere orientation angle ϕ is 30° (Fig. 8c) and the maximum height of the relief is about 1 nm ($\pm$ 0·2 nm). This may represent an underestimation of the total corrugation depth, since the tip geometry may have prevented the tip from truly probing the bottom of the depressions between capsomeres (Amrein *et al.*, 1989). For TEM, polyheads were rotary shadowed at an elevation angle of 30° (Fig. 9). The film appears fine grained and the periodic structure is revealed by its relief contrast. The average capsomere morphology (Fig. 9b) compares well with STM data (Fig. 8c). The positions of the protomers coincide well with those revealed in STM images. On the threefold axis, the three neighbouring protomers are connected by fine Y-shaped structures ('3' in Fig. 9b), whereas on the twofold axis, the protomers show X-shaped interconnections ('2' in Fig. 9b). The capsomere orientation angle is 31°

Figure 10(a) shows an SE image of a Pt/Ir/C-coated polyhead imaged in an in-lens type FESEM. When image averaging is applied, the best resolution was obtained with a film thickness of 1·5 nm. In the SE mode the fine grains appear with a high signal surrounded by a diffuse background. The capsomeres are just visible in the micrograph. With thicker Pt/Ir/C films the capsomeres become directly visible but after averaging the highest possible resolution is lost. In the averaged image the hexameric structure is well resolved and even the Y-shaped connections are faintly visible. The arrangement of the protomers compares well with TEM and STM data. TEM and SEM reveal more details from the lower part of the relief than STM measurements, most probably because the shape of the tunnelling tip has prevented it from probing these structures. The measured capsomere orientation angle ϕ of 30–31° is the same for all three surface imaging methods. Averaged capsomeres of negatively stained type III polyheads, however, reveal an orientation angle ϕ of 21° (Steven *et al.*, 1976). This difference is probably due to the fact that TEM images of negatively stained specimens represent a through-projection of the whole stain-excluding mass, whereas STM, SEM and TEM images of metal-coated specimens are surface representations. Thus, if the protomer is an elongated structure with the corresponding axis being tilted relative to a normal to the specimen support, then the two orientation angles will differ.

CONCLUSIONS

The carbon content of Pt/Ir/C films may be chosen within a range of 20–70%. Pt/Ir/C films that contain at least 25% carbon remain intact upon transfer to atmospheric conditions and allow high-resolution features of macromolecular structures to be preserved in SEM and STM, as well as in TEM. Most probably, Pt/Ir/C films cannot entirely preserve the overall shape at organelle and cellular dimensions. Here water contributes as a major structure-forming element and its removal, even by careful freeze-drying, may result in collapse. For high structural preservation of such cryo-fixed material, the structures have to be coated at a partially frozen hydrated stage and cryo-transferred under high vacuum conditions into the SEM, equipped with a cold stage.

The grain size of Pt/Ir/C films is reduced when compared to Pt/C films. This is a consequence of a higher carbon incorporation into the coating film where carbon acts as a diffusion barrier. We therefore suggest that Pt/Ir/C films are composed of an amorphous carbon layer that contains small isolated metal clusters.

The film thickness of 1·5 nm required for 3-D stability may limit the resolution of biological structures in TEM and STM. In SEM, this film thickness applied on a freeze-dried polyhead gave optimal resolution after image processing. Further investigations on thicker structures have to prove the Pt/Ir/C film qualities and its signal formation in SEM. The polyhead surface showed that the same arrangement of the protomeres can be obtained in TEM, STM and SEM imaging. However, TEM and SEM revealed more detail from the lower part of the relief than STM measurements, such as two different types of interconnections between the capsomeres. On the other hand, the major advantage of STM is the direct and precise height measurement. In the case of polyheads an apparent surface topography of only 1 nm was resolved.

For structural research it will become more and more important to combine structural information from basically different imaging approaches. From this point of view it is very important to get an even better understanding of the relation between a coated surface relief and the contrast obtained in TEM, STM and SEM.

ACKNOWLEDGMENTS

We are grateful to Drs Ueli Aebi, Eduard Kellenberger and Andreas Engel for providing us with polyheads. We also thank Dr Wolfgang Baumeister for providing us with the HPI-layer. We would like to thank Dr René Hermann for SEM imaging, and Prof. Hans Moor and Dr Martin Müller for continuous support. We benefited from the technical assistance of Peter Tittmann and Katherina Krusche and we wish to thank Gustav Bellin and Tom Lotto for the photographic work. Last, but not least, we thank Mrs Deirdre Gilligan for corrections to the English.

REFERENCES

Amrein, M., Dürr, R., Winkler, H., Travaglini, G., Wepf, R. & Gross, H. (1989) STM of freeze-dried and Pt–Ir–C coated bacteriophage T4 Polyheads. *J. Ultrastruct. Res.* **102,** 170–177.

Amrein, M., Stasiak, A., Gross, H., Stoll, E. & Travaglini, G. (1988) Scanning tunneling microscopy of recA-DNA complexes coated with a conducting film. *Science,* **240,** 514–516.

Bachmann, L., Abermann, R. & Zingsheim, H.P. (1969) Hochauflösende Gefrierätzung. *Histochemistry,* **20,** 133–142.

Bachmann, L., Becker, R., Leupold, G., Barth, M., Guckenberger, R. & Baumeister, W. (1985) Decoration and shadowing of freeze-etched catalase crystals. *Ultramicroscopy,* **16,** 305–320.

Bachmann, L. & Hilbrand, H. (1965) Sinterung von Aufdampfschichten aus Silber und Gold unter dem Einfluss von Adsorptionsschichten. *Grundprobleme der Physik dünner Schichten* (ed. by R. Niedermayer and H. Mayer), pp. 77–82. Vandenhoeck, Rupprecht, Göttingen.

Baumeister, W., Bart, M., Hegerl, R., Guckenberger, R., Hahn, M. & Saxton, W.O. (1986) Three-dimensional structure of the regular surface layer (HPI-layer) of *Deinococcus radiodurans. J. Mol. Biol.* **187,** 241–253.

Baumeister, W., Karrenberg, F., Rachel, R., Engel, A., Ten Heggeler, B. & Saxton, W.O. (1982) The major cell envelope protein of *Micrococcus radiodurans* (R1). *Eur. J. Biochem.* **125,** 535–544.

Bradley, D.E. (1958) High resolution evaporation of Pt and carbon for possible use in high-resolution shadowing-casting for the electron microscope. *Nature,* **181,** 875–877.

Buhle, E.L., Aebi, U. & Smith, P.R. (1985) Correlation of surface topography of metal-shadowed specimens with their negatively stained reconstructions. *Ultramicroscopy,* **16,** 436–450.

Echlin, P. (1968) The use of the scanning reflection electron microscope in the study of plant and microbial material. *J. R. Microsc. Soc.* **88,** 407–418.

Gerber, C., Binnig, G., Fuchs, H., Marti, O. & Rohrer, H. (1986) Scanning tunneling microscope combined with a scanning electron microscope. *Rev. Sci. Instrum.* **57,** 221–226.

Gross, H. (1987) High resolution metal replication of freeze-dried specimen. *Cryotechniques in Biological Electron Microscopy* (ed. by R. A. Steinbrecht and K. Zierold), pp. 205–215. Springer-Verlag, Berlin.

Gross, H., Müller, T., Wildhaber, I. & Winkler, H. (1985) High resolution metal replication, quantified by image processing of periodic test specimens. *Ultramicroscopy,* **16,** 287–304.

Guckenberger, R., Kösslinger, C., Gatz, R., Breu, H., Levai, N. & Baumeister, W. (1988) A scanning tunneling microscope (STM) for biological applications: design and performance. *Ultramicroscopy*, **25**, 111–122.

Hoenger, A., Gross, H., Aebi, U. & Engel, A. (1990) Localization of the lipopolysaccharides in metal-shadowed reconstituted lipid–porin membranes. *J. Struct. Biol.* **103**, 185–195.

Jakubowski, U., Hegerl, R., Formanek, H., Volker, U., Santarius, U. & Baumeister, W. (1988) Three-dimensional reconstruction of the HPI-layer of *Deinococcus radiodurans* embedded in Cd-thioglycerol. *Proc. EUREM*, **3**, 381–382.

Knoch, M. & König, H. (1956) Strukturlose Platinabdrücke biologischer Objekte. *Z. Wiss. Mikr.* **63**, 121–130.

Mahl, H. (1942) Die übermikroskopische Oberflächendarstellung mit dem Abdruckverfahren. *Naturwiss.* **30**, 207–217.

McMullen, D. (1989) SEM—past, present and future. *J. Microsc.* **155**, 373–392.

Müller, H.O. (1942) Die Ausmessung der Tiefe übermikroskopischer Objekte. *Kolloid Z.* **99**, 6–28.

Nagatani, T., Saito, S., Sato, M. & Yamada, M. (1987) Development of an ultra high resolution scanning electron microscope by means of a field emission source and in-lens system. *Scanning Microsc.* **1**, 901–909.

Oda, Y. & Nakajima, K. (1975) Quantitative electron probe microanalysis of thin films. *Trans. JIM*, **16**, 697–701.

Peters, K.R. (1986) Metal deposition by high-energy sputtering for high magnification electron microscopy. *Advanced Technique in Biological Electron Microscopy* (ed. by J. K. Koehler), pp. 101–166. Springer-Verlag, Berlin.

Reimer, L. (1967) *Elektronenmikroskopische Untersuchungs- und Präperationsmethoden.* Springer-Verlag, Berlin.

Saxton, W.O. & Baumeister, W. (1982) The correlation averaging of a regularly arranged bacterial cell envelope protein. *J. Microsc.* **127**, 127–138.

Skatulla, W. & Horn, L. (1960) Ein einfaches, hochauflösendes Abdruckverfahren für die Elektronenmikroskopie. *Exp. Tech. Phys.* **8**, 1–9.

Smith, K.C. & Oatley, M.A. (1955) The scanning electron microscope and its field of application. *Brit. J. Appl. Phys.* **6**, 391–399.

Stemmer, A., Hefti, A. & Engel, A. (1989) Scanning tunneling and transmission electron microscopy on identical areas of biological specimens. *Ultramicroscopy*, **30**, 263–280.

Steven, A.C., Couture, E., Aebi, U. & Showe, M.K. (1976) Structure of T4 Polyheads. *J. Mol. Biol.* **106**, 187–221.

Venables, J.A., Spiller, G.D.T. & Hanbücken, M. (1984) Nucleation and growth of thin films. *Rep. Prog. Phys.* **47**, 399–459.

Walther, P. & Hentschel, J. (1989) Improved representation of cell surface structures by freeze substitution and backscattered electron imaging. *Scanning Microsc.* **3**, 201–211.

Williams, R.C. & Wyckoff, R.W.G. (1944) The thickness of electron microscopy objects. *J. Appl. Phys.* **15**, 712–716.

Winkler, H., Gross, H., Schnyder, T. & Kunath, W. (1991) Circular harmonic averaging of rotary-shadowed and negatively stained creatine kinase macromolecules. *J. Electron Microsc. Technique*, **18** (in press).

Winkler, H., Wildhaber, I. & Gross, H. (1985) Decoration effects on the surface of a regular protein layer. *Ultramicroscopy*, **16**, 331–339.

Zasadzinsky, J.A.N., Schneir, J., Gurley, J., Elings, V. & Hansma, P.K. (1988) Scanning tunneling microscopy of replicas of biomembranes. *Science*, **239**, 1014–1016.